Stretchable living materials and devices with hydrogel–elastomer hybrids hosting programmed cells

Xinyue Liu[a,1], Tzu-Chieh Tang[b,c,1], Eléonore Tham[b,d,1], Hyunwoo Yuk[a,1], Shaoting Lin[a], Timothy K. Lu[b,c,e,2], and Xuanhe Zhao[a,f,2]

[a]Soft Active Materials Laboratory, Department of Mechanical Engineering, Massachusetts Institute of Technology, Cambridge, MA 02139; [b]Synthetic Biology Group, Research Laboratory of Electronics, Massachusetts Institute of Technology, Cambridge, MA 02139; [c]Department of Biological Engineering, Massachusetts Institute of Technology, Cambridge, MA 02139; [d]Department of Materials Science and Engineering, Massachusetts Institute of Technology, Cambridge, MA 02139; [e]Department of Electrical Engineering and Computer Science, Massachusetts Institute of Technology, Cambridge, MA 02139; and [f]Department of Civil and Environmental Engineering, Massachusetts Institute of Technology, Cambridge, MA 02139

Living systems, such as bacteria, yeasts, and mammalian cells, can be genetically programmed with synthetic circuits that execute sensing, computing, memory, and response functions. Integrating these functional living components into materials and devices will provide powerful tools for scientific research and enable new technological applications. However, it has been a grand challenge to maintain the viability, functionality, and safety of living components in freestanding materials and devices, which frequently undergo deformations during applications. Here, we report the design of a set of living materials and devices based on stretchable, robust, and biocompatible hydrogel–elastomer hybrids that host various types of genetically engineered bacterial cells. The hydrogel provides sustainable supplies of water and nutrients, and the elastomer is air-permeable, maintaining long-term viability and functionality of the encapsulated cells. Communication between different bacterial strains and with the environment is achieved via diffusion of molecules in the hydrogel. The high stretchability and robustness of the hydrogel–elastomer hybrids prevent leakage of cells from the living materials and devices, even under large deformations. We show functions and applications of stretchable living sensors that are responsive to multiple chemicals in a variety of form factors, including skin patches and gloves-based sensors. We further develop a quantitative model that couples transportation of signaling molecules and cellular response to aid the design of future living materials and devices.

hydrogels | synthetic biology | genetically engineered bacteria | biochemical sensors | wearable devices

G enetically engineered cells enabled by synthetic biology have accomplished multiple programmable functions, including sensing (1), responding (2), computing (3), and recording (4). Powered by this emerging capability to program cells into living computers (1–6), the integration of genetically encoded cells into freestanding materials and devices will not only provide new tools for scientific research but also, lead to unprecedented technological applications (7). However, the development of such living materials and devices has been significantly hampered by the demanding requirements for maintaining viable and functional cells in materials and devices plus biosafety concerns toward the release of genetically modified organisms into environments. For example, gene networks embedded in paper matrices have been used for low-cost rapid viruses detection and protein manufacturing (1). However, their gene networks are based on freeze-dried extracts from genetically engineered cells to operate, partially because the paper substrates cannot sustain long-term viability and functionality of living cells or prevent their leakage. As another example, by seeding cardiomyocytes on thin elastomer films, biohybrid devices have been developed as soft actuators (8) and biomimetic robots (9). However, because the cells are not protected or isolated from the environment, the biohybrid devices need to operate in media, and the cells may detach from the elastomer films. Thus, it remains a grand challenge to integrate genetically encoded cells into

practical materials and devices that can maintain long-term viability and functionality of the cells, allow for efficient chemical communications between cells and with external environments, and prevent cells from escaping the materials or devices. A versatile material system and a general method to design living materials and devices capable of diverse functions (1, 8–10) remain a critical need in the field.

As polymer networks infiltrated with water, hydrogels have been widely used as scaffolds for tissue engineering (11) and vehicles for cell delivery (12) owing to their high water content, biocompatibility, biofunctionality, and permeability to a wide range of chemicals and biomolecules (13). The success of hydrogels as cell carriers in tissue engineering and cell delivery shows their potential as an ideal matrix for living materials and devices to incorporate genetically engineered cells. However, common hydrogels exhibit low mechanical robustness (14) and difficulty in bonding with other materials and devices (15), which have posed challenges in using them as matrices for living materials and devices (10). Significant progress has been made toward designing hydrogels with high mechanical toughness and stretchability (14, 16, 17) and robustly bonding hydrogels to engineering materials, such as glass, ceramics, metals, and elastomers (15, 18, 19). Combining programmed cells with robust biocompatible hydrogels has the potential to enable an avenue to create new living materials and devices, but this promising approach has not been explored yet.

Here, we show the design of a set of living materials and devices based on stretchable, robust, and biocompatible hydrogel–elastomer

Significance

The integration of genetically programmed cells into materials and devices will enable the power of biology to be harnessed for a wide range of scientific research and technological applications. Here, we use stretchable, robust, and biocompatible hydrogel–elastomer hybrids to host genetically programed bacteria, thus creating a set of stretchable and wearable living materials and devices that possesses unprecedented functions and capabilities. A quantitative yet generic model is further developed to account for the coupled physical and biochemical processes in living materials and devices. This simple strategy for designing living materials and devices not only provides tools for research in synthetic biology but also, enables applications, such as living sensors, interactive genetic circuits, and living wearable devices.

hybrids that host various types of genetically engineered bacterial cells. We show that our hydrogels can sustainably provide water and nutrients to the cells, whereas our elastomers ensure sufficient air permeability to maintain viability and functionality of the bacteria. Communication between different types of genetically engineered cells and with the environment is achieved via transportation of signaling molecules in hydrogels. The high stretchability and robustness of the hydrogel–elastomer hybrids prevent leakage of cells from the living materials and devices under repeated deformations. We show applications uniquely enabled by our living materials and devices, including stretchable living sensors responsive to multiple chemicals, interactive genetic circuits, a living patch that senses chemicals on the skin, and a glove with living chemical detectors integrated at the fingertips. A quantitative model that couples transportation of signaling molecules and responses of cells is further developed to help the design of future living materials and devices.

Results

Design of Living Materials and Devices. We propose that encapsulating genetically engineered cells in biocompatible, stretchable, and robust hydrogel–elastomer hybrid matrices represents a general strategy for the design of living materials and devices with powerful properties and functions. The design of a generic structure for the living materials and devices is illustrated in Fig. 1A. In brief, layers of robust and biocompatible hydrogel and

Fig. 1. Design of living materials and devices. (A) Schematic illustration of a generic structure for living materials and devices. Layers of robust and biocompatible hydrogel and elastomer were assembled and bonded into a hybrid structure, which can transport sustained supplies of water, nutrient, and oxygen to genetically engineered cells at the hydrogel–elastomer interface. Communication between different types of cells and with the environment was achieved by diffusion of small molecules in hydrogels. (B) Schematic illustration of the high stretchability and high robustness of the hydrogel–elastomer hybrids that prevent cell leakage from the living device, even under large deformations. Images show that the living device can sustain uniaxial stretching over 1.8 times and twisting over 180° while maintaining its structural integrity. (C) Viability of bacterial cells at room temperature over 3 d. The cells were kept in the device placed in the humid chamber without additional growth media (yellow), in the device immersed in the growth media as a control (green), and in growth media as another control (black; $n = 3$ repeats). (D) OD_{600} and (Insets) streak plate results of the media surrounding the defective devices (yellow) and intact devices at different times after 1 (black) or 500 times (green) deformation of the living devices and immersion in media ($n = 3$ repeats).

elastomer were assembled and bonded into a hybrid structure (15). Patterned cavities of different shapes and sizes were introduced on the hydrogel–elastomer interfaces to host living cells in subsequent steps. The hydrogel–elastomer hybrid was then immersed in culture media for 12 h, so that the hydrogel can be infiltrated with nutrients. Thereafter, genetically engineered bacteria suspended in media were infused into the patterned cavities through the hydrogel, and the injection points were then sealed with drops of fast-curable pregel solution (Fig. S1). Because the hydrogel was infiltrated with media and the elastomer is air-permeable, hydrogel–elastomer hybrids with proper dimensions can provide sustained supplies of water, nutrient, and oxygen (if needed) to the cells. By tuning the dimensions of hydrogel walls between different types of cells and between cells and external environments, we can control the transportation times of signaling molecules for cell communication. Furthermore, the high mechanical robustness of the hydrogel, elastomer, and their interface confers structural integrity to the matrix even under large deformations, thus preventing cell escape in dynamic environments.

In this study, we chose polyacrylamide (PAAm)-alginate hydrogel (15, 17) and polydimethylsiloxane (Sylgard 184; Dow Corning) or Ecoflex (Smooth-On) silicone elastomer to constitute the robust hydrogel and elastomer, respectively. The biocompatibility of these materials has been extensively validated in various biomedical applications (20, 21). The sufficient gas permeation of the silicone elastomer enables oxygen supply for the bacteria (22–24). If a higher level of oxygen is required, one may choose elastomers with higher permeability, such as Silbione (25), or microporous elastomers (23). In the hydrogel, the covalently cross-linked PAAm network is highly stretchable, and the reversibly cross-linked alginate network dissipates mechanical energy under deformation, leading to tough and stretchable hydrogels (14, 17, 26). More robust devices can be fabricated by using fiber-reinforced tough hydrogel (27). Robust bonding between the hydrogel and elastomer can be achieved by covalently anchoring the PAAm network on the elastomer substrate (15, 18, 26). The Escherichia coli bacterial strains were engineered to produce outputs [e.g., expressing GFP (green fluorescent protein)] under control of promoters that are inducible by cognate chemicals. For example, the 2,4-diacetylphloroglucinol$_{Receiver}$ (DAPG$_{RCV}$)/GFP strain produces GFP when the chemical inducer DAPG is added and received by the cells. The cell strains used in this study included DAPG$_{RCV}$/GFP, N-acyl homoserine lactone$_{RCV}$ (AHL$_{RCV}$)/GFP, isopropyl β-D-1-thiogalactopyranoside$_{RCV}$ (IPTG$_{RCV}$)/GFP, rhamnose$_{RCV}$ (Rham$_{RCV}$)/GFP, and anhydrotetracycline$_{RCV}$ (aTc$_{RCV}$)/AHL. The DAPG, AHL, IPTG, Rham, and aTc are small molecules with biochemical activities and used as the signaling molecules in this study.

To evaluate the viability of cells in living materials and devices, we placed the hydrogel–elastomer matrices containing Rham$_{RCV}$/GFP cells (Fig. 1A) in a humid chamber (relative humidity > 90%) without addition of growth media or immersed the living materials in the growth media at room temperature (25 °C) for 3 d. We also directly cultured the cells in growth media as a control. Thereafter, we used the live/dead stain and performed flow cytometry analysis for bacteria retrieved from the living device to test the cell viability. As shown in Fig. 1C and Fig. S2, the viability of cells in the device placed in a humid chamber maintains above 90% over 3 d without addition of media to the device. This viability is similar to that of cells in the device immersed in media or cells directly cultured in media at room temperature over 3 d.

To test whether bacteria could escape from the living devices, we deformed the hydrogel–elastomer hybrids containing Rham$_{RCV}$/GFP bacteria in different modes (i.e., stretching and twisting) as illustrated in Fig. 1B, and then immersed the device in media for a 24-h period. As shown in Fig. 1B and Fig. S3, the living device made of Ecoflex and tough hydrogel sustained a uniaxial stretch over 1.8 times its original length and a twist over 180° while maintaining its structural integrity. Furthermore, after immersing the device in media for 6, 12, 20, and 24 h, we collected the media surrounding the device and measured the cell
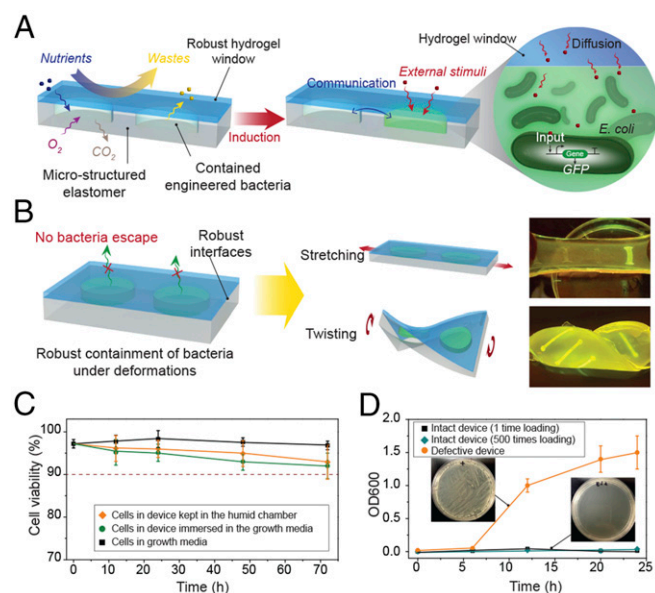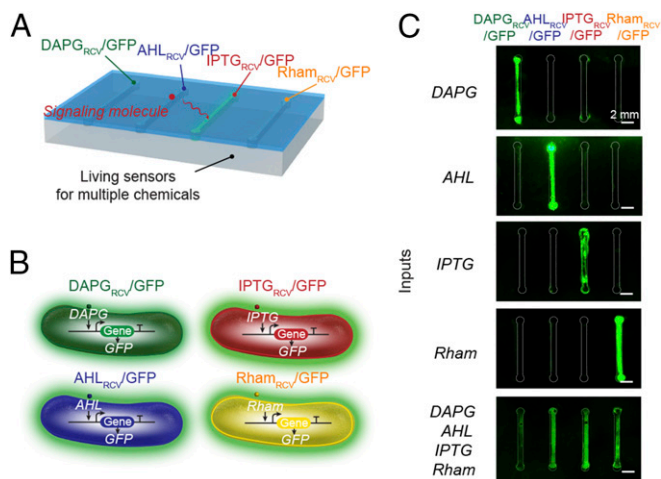
Fig. 2. Stretchable living sensors can independently detect multiple chemicals. (A) Schematic illustration of a hydrogel–elastomer hybrid with four isolated chambers to host bacterial strains, including DAPG$_{RCV}$/GFP, AHL$_{RCV}$/GFP, IPTG$_{RCV}$/GFP, and Rham$_{RCV}$/GFP. Signaling molecules were diffused from the environment through the hydrogel window into cell chambers, where they were detected by the bacteria. (B) Genetic circuits were constructed in bacterial strains to detect cognate inducers (i.e., DAPG, AHL, IPTG, and Rham) and produce GFP. (C) Images of living devices after exposure to individual or multiple inputs. Cell chambers hosting bacteria with the cognate sensors showed green fluorescence, whereas the noncognate bacteria in chambers were not fluorescent. Scale bars are shown in images.

population in the media over time via OD$_{600}$ by UV spectroscopy (Fig. 1D); 200 μL media were streaked on agar plates after 24 h to check for cell escape and growth (Fig. 1D, Insets). Fig. 1D shows that bacteria did not escape the hydrogel–elastomer hybrid even under repeated mechanical loads (500 cycles). As controls, we intentionally created defective devices (with weak hydrogel–elastomer bonding) and observed significant escape and overgrowth of bacteria after immersing the samples in media (yellow curve in Fig. 1D). Because agar hydrogels have been widely used for cell encapsulation, we fabricated an agar-based control device that encapsulated Rham$_{RCV}$/GFP bacteria with the same dimensions as the hydrogel–elastomer hybrid. In Fig. S4, it can be seen that these agar devices underwent failures even under moderate deformation (e.g., a stretch of 1.1 or a twist of 60°). Moreover, cell leakage from the agar devices occurred regardless of the presence of any deformation, likely because of the large pore sizes and sol–gel transition of the agar gel, allowing for escape of encapsulated bacteria (Fig. S5). These results indicate that our hydrogel–elastomer hybrids can provide a biocompatible, stretchable, and robust host for genetically engineered bacteria.

Stretchable Living Sensors for Chemical Sensing. We next show functions and applications enabled by the living materials and devices. Fig. 2A illustrates a hydrogel–elastomer hybrid with four isolated chambers that each hosted a different bacterial strain: DAPG$_{RCV}$/GFP, AHL$_{RCV}$/GFP, IPTG$_{RCV}$/GFP, and Rham$_{RCV}$/GFP. The genetic circuits in these bacterial strains can sense their cognate inducers and express GFP (Fig. S6), which can be visible under blue light illumination. As mentioned above, the DAPG$_{RCV}$/GFP strain exhibits green fluorescence when receiving DAPG but is not responsive to other stimuli. Similarly, the AHL$_{RCV}$/GFP strain expresses GFP only induced by AHL, IPTG selectively induces GFP expression in the IPTG$_{RCV}$/GFP strain, and Rham selectively induces the green fluorescence output of the Rham$_{RCV}$/GFP strain (Fig. 2B). We show that each inducer, diffusing from the environment through the hydrogel into cell chamber, can trigger GFP expression of its cognate strain inside the device, which could be visualized by the naked eye or microscope (Fig. 2C and

Fig. S7). This orthogonality makes the hydrogel–elastomer hybrid with encapsulated bacteria into a living sensor that can simultaneously detect multiple chemicals in the environment (Fig. 2C). About 2 h are required for each strain to produce significant fluorescence. Parameters that affect response times for the living sensor are discussed with a quantitative model below.

Interactive Genetic Circuits. Next, we integrated cells containing different genetic circuits into a freestanding living device to study cellular signaling cascades. We designed two bacterial strains that can communicate via the diffusion of signaling molecules through the hydrogel, although both were separated by an elastomer barrier within discrete chambers of the device (Fig. 3A). Specifically, we used a transmitter strain (aTc$_{RCV}$/AHL) that produces the quorum-sensing molecule AHL when induced by aTc and a receiver strain (AHL$_{RCV}$/GFP) with AHL-inducible GFP genes (5). We triggered this device with aTc from the environment to induce the transmitter cells, which resulted in AHL production and stimulation of receiver cells to synthesize GFP (Fig. 3C). In Fig. 3B, we plot the normalized fluorescence of bacteria in different cell chambers (i.e., transmitter and receiver in Fig. 3A) as a function of time after aTc was added outside the device. Because there is no GFP gene in the transmitter cells (aTc$_{RCV}$/AHL), their chambers showed no fluorescence over time
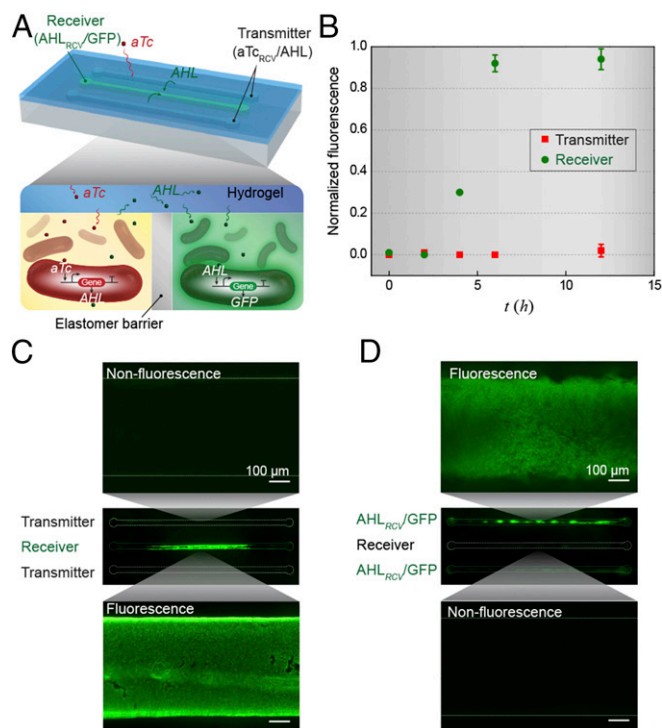

Fig. 3. Interactive genetic circuits. (A) Schematic illustration of a living device that contains two cell strains: the transmitters (aTc$_{RCV}$/AHL strain) produce AHL in the presence of aTc, and the receivers (AHL$_{RCV}$/GFP strain) express GFP in the presence of AHL. The transmitters could communicate with the receivers via diffusion of the AHL signaling molecules through the hydrogel window, although the cells are physically isolated by elastomer. (B) Quantification of normalized fluorescence over time ($n = 3$ repeats). All data were measured by flow cytometry, with cells retrieved from the device at different times. (C) Images of device and microscopic images of cell chambers 6 h after addition of aTc into the environment surrounding the device. The side chambers contain transmitters, whereas the middle one contains receivers. (D) Images of device and microscopic images of cell chambers 6 h after aTc addition in the environment. The side chambers contain aTc$_{RCV}$/GFP instead of transmitters, whereas the middle one contains receivers. Scale bars are shown in images.

(Fig. 3B). It took longer response time (∼5 h) for the receiver cells in the middle chamber to exhibit significant fluorescence compared with the cells in simple living sensors (Fig. 2A). Two diffusion processes (i.e., aTc from the environment to the two side chambers and AHL from the two side chambers to the central chamber) and two induction processes (i.e., AHL production induced by aTc in transmitters and GFP expression induced by AHL in receivers) were involved in the current interactive genetic circuits. As a control, when the transmitters (aTc$_{RCV}$/AHL) in the device were replaced by a cell strain containing aTc-inducible GFP (aTc$_{RCV}$/GFP) that cannot communicate with AHL$_{RCV}$/GFP, no fluorescence was observed in the receiver (AHL$_{RCV}$/GFP) chamber (Fig. 3D). Overall, the integrated devices containing interactive genetic circuits provide a platform for the detection of various chemicals and the investigation of cellular interaction among physically isolated cell populations.

Living Wearable Devices. To further show practical applications of living materials and devices, we fabricated a living wearable patch that detects chemicals on the skin (Fig. 4 A–D). The sensing patch matrix consists of a bilayer hybrid structure of tough hydrogel and silicone elastomer. The wavy cell channels could cover a larger area of the skin with a limited amount of bacterial cells (Fig. 4A). The living patch can be fixed on the skin by clear Scotch tape, with the hydrogel exposed to the skin and the elastomer exposed to the air. The compliance and stickiness of the hydrogel promote conformal attachment of the living patch to human skin, whereas the silicone elastomer cover effectively prevents the dehydration of the sensor patch (Fig. S8) (15). As shown in Fig. 4 B–D, the inducer Rham was smeared on the skin of a forearm before we adhered the living patch. The channels with Rham$_{RCV}$/GFP in the living patch became fluorescent within 4 h, whereas channels with AHL$_{RCV}$/GFP did not show any difference. As controls, no fluorescence was observed in any channels in absence of any inducer on the skin (Fig. S9A), whereas all channels became fluorescent in presence of both AHL and Rham (Fig. S9B). Although the inducers are used as mock biomarkers here, more realistic chemical detections, such as components in human sweat or blood, may be pursued with living devices for scientific research and translational medicine in the future.

As another application, a glove with chemical detectors integrated at the fingertips was fabricated (Fig. 4E). The stretchable hydrogel and tough bonding between hydrogel and rubber allow for robust integration of living monitors on flexible gloves. To show the capability of this living glove, a glove-wearer held cotton balls that have absorbed inducers. Those chemicals from the cotton ball would diffuse through the hydrogel and induce fluorescence in the engineered bacteria (Fig. 4 F–H). For example, gripping a wet cotton ball that contained IPTG and Rham resulted in fluorescence at two of three bacterial sensors that contained IPTG$_{RCV}$/GFP (Fig. 4 G and H, *) and Rham$_{RCV}$/GFP (Fig. 4 G and H, ***) on the glove within 4 h. The middle sensor containing AHL$_{RCV}$/GFP (Fig. 4 G and H, **) remained unaffected. The living patch and biosensing glove show the potential of living materials as low-cost and mechanically flexible platforms for healthcare and environmental monitoring. Looking forward, we envision the design of living devices that can be wearable, ingestible, or implantable for applications, such as water quality alert, disease diagnostics, and therapy.

Discussion and Modeling

Model of Living Materials and Devices. In this section, we developed a model that quantitatively accounted for the coupled physical transportation and biochemical responses underlying the living sensor (Fig. 2). The operation of the living sensor (Fig. 2A) relied on two processes: diffusion of signaling molecules from the environment through the hydrogel window into cell chambers and induction of the encapsulated cells by the signaling molecules (28). Given the geometry of the senor (Fig. 5A), we could
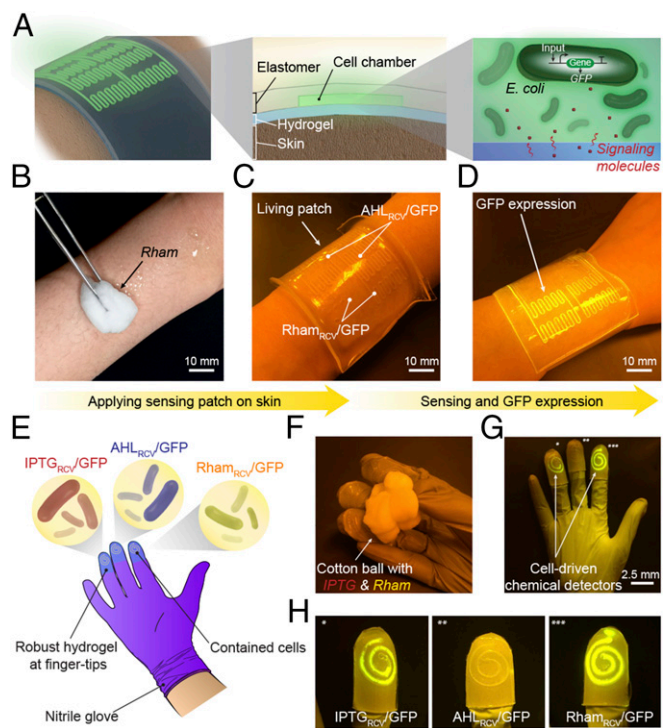

Fig. 4. Living wearable devices. (A) Schematic illustration of a living patch. The patch adhered to the skin with the hydrogel side, and the elastomer side was exposed to the air. Engineered bacteria inside can detect signaling molecules. (B–D) Rham solution was smeared on skin, and the sensor patch was conformably applied on skin. The channels with Rham$_{RCV}$/GFP in the living patch became fluorescent, whereas channels with AHL$_{RCV}$/GFP did not show any differences. Scale bars are shown in images. (E) Schematic illustration of a glove with chemical detectors robustly integrated at the fingertips. Different chemical-inducible cell strains, including IPTG$_{RCV}$/GFP, AHL$_{RCV}$/GFP, and Rham$_{RCV}$/GFP, were encapsulated in the chambers. (F–H) When the living glove was used to grab a wet cotton ball containing the inducers, GFP fluorescence was shown in the cognate sensors IPTG$_{RCV}$/GFP (*) and Rham$_{RCV}$/GFP (***) on the gloves. In contrast, the noncognate sensor AHL$_{RCV}$/GFP (**) did not show any fluorescence. Scale bars are shown in images.

approximate the transportation of inducer in the hydrogel and the cell chamber to follow the 1D Fick's law:

$$\frac{\partial I}{\partial t} = D_g \frac{\partial^2 I}{\partial x^2} \quad \text{for} \quad 0 \le x < L_g \tag{1}$$

and

$$\frac{\partial I}{\partial t} = D_c \frac{\partial^2 I}{\partial x^2} \quad \text{for} \quad L_g \le x < L_g + L_c, \tag{2}$$

where x is the coordinate of a point in the hydrogel window or the cell chamber; L_g and L_c are the thicknesses of the hydrogel and cell chamber, respectively; t is the current time; I is the inducer concentration in hydrogel or medium in the cell chamber; and D_g and D_c are the diffusion coefficients of the inducer in hydrogel and medium, respectively.

To prescribe boundary conditions for Eqs. 1 and 2, the inducer concentration at the boundary between the environment and the hydrogel window is taken to be a constant I_0, the inducer concentration and inducer flux are taken to be continuous across the interface between the hydrogel and cell chamber, and the elastomer wall of the cell chamber is taken to be impermeable to the inducers. Because the diffusion process begins at $t = 0$, the inducer concentration throughout the hydrogel window and cell
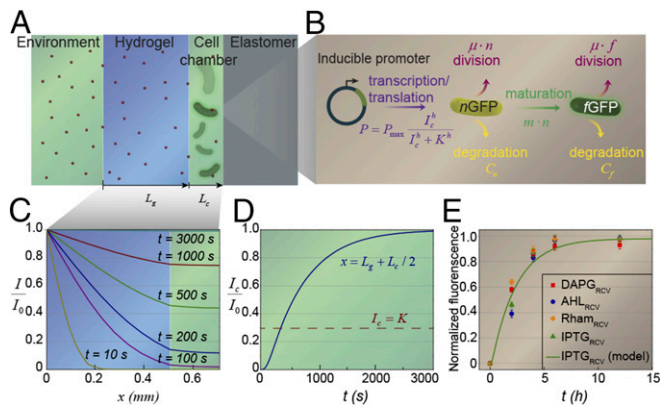
Fig. 5. Model for the diffusion–induction process in living materials and devices. (*A*) Schematic illustration of the diffusion of signaling molecules from the environment through the hydrogel to cell chambers in the living device. (*B*) Diagram of GFP expression after induction with a small molecule chemical. (*C*) Inducer concentration profile throughout the hydrogel window and cell chamber at different times. (*D*) Typical inducer concentration in the cell chamber as a function of time. (*E*) The normalized fluorescence of different cell strains as a function of time after addition of inducer ($n = 3$ repeats). Dots represent experimental data, and curve represents the model.

chamber is zero when $t \leq 0$ as the initial condition for Eqs. **1** and **2**. Furthermore, the consumption of inducers by the bacterial cells was taken to be negligible. In these experiments, we set $L_g = 5 \times 10^{-4}$ m, $L_c = 2 \times 10^{-4}$ m, and $I_0 = 1$ mM for IPTG diffusion–induction. The diffusion coefficients of inducers are estimated to be $D_g = 3 \times 10^{-10}$ m²/s and $D_c = 1 \times 10^{-9}$ m²/s based on previous measurements (29).

The diffusion equations together with boundary and initial conditions were solved numerically. In Fig. 5*C*, we plot the inducer concentrations throughout the hydrogel window and cell chamber at different times. It can be seen that the distribution of inducers in the cell chamber is more uniform than that in the hydrogel because of the higher inducer diffusion coefficient in media than that in hydrogel. We further define the typical inducer concentration I_c as the inducer concentration at the center of the cell chamber [i.e., $I_c = I(t, x = L_g + L_c/2)$]. In Fig. 5*D*, we plot the typical inducer concentration in the cell chamber as a function of time.

To characterize the GFP expression of the bacterial cells in the living sensor, we adopt a model from Leveau and Lindow (30). The inducers can bind with repressors or activators in a bacterial cell and induce the transcription of promoters. The induced promoters initiate the synthesis of nonfluorescent GFP (^{n}GFP). Meanwhile, the ^{n}GFP in the cell is consumed because of the maturation into the fluorescent GFP (^{f}GFP), cell division, and protein degradation. The converted ^{f}GFP also undergoes consumption because of cell division and protein degradation. Eventually, the syntheses and consumptions of ^{n}GFP and ^{f}GFP reach steady states in the cell (Fig. 5*B*). Denoting the numbers of ^{n}GFP and ^{f}GFP in a cell as n and f, respectively, their rates of variation can be approximated as

$$\frac{\partial n}{\partial t} = P - m \cdot n - \mu \cdot n - C_n \qquad \qquad [3]$$

and

$$\frac{\partial f}{\partial t} = m \cdot n - \mu \cdot f - C_f. \qquad \qquad [4]$$

In Eqs. **3** and **4**, P is the promoter activity that expresses ^{n}GFP; $m \cdot n$ prescribes the maturation rate of ^{n}GFP into ^{f}GFP, where m is the maturation constant; $\mu \cdot n$ and $\mu \cdot f$ prescribe the consumption rates of ^{n}GFP and ^{f}GFP caused by cell division, respectively,

where μ is the growth constant; and C_n and C_f are the degradation rates of ^{n}GFP and ^{f}GFP, respectively. The promoter activity for transcription and translation induced by an inducer is approximated by a Hill equation (31) $P = P_{max} I^h / (I^h + K^h)$, in which P_{max} is the maximum rate of ^{n}GFP expression (i.e., maximum promoter activity), h is the Hill coefficient, and K is the half-maximal parameter (inducer concentration at which P equals $0.5 P_{max}$). Because the inducer concentration in the cell chamber is relatively uniform (Fig. 5*C*), we take I in the promoter activity expression to be the typical concentration in the cell chamber (i.e., $I = I_c$). Evidently, the connection between the transportation of inducers and biochemical responses of cells in the living sensor is through this Hill equation. Because the half-life of GFP in *E. coli* is over 24 h in absence of any proteolytic degradation, much longer than the typical responsive time of the living sensor, we assume $C_n = C_f = 0$ throughout this study. For the IPTG$_{RCV}$/GFP strain, we take $P_{max} = 1,000$ s⁻¹, $K = 0.3$ mM, $h = 2$, $m = 1.16 \times 10^{-2}$ s⁻¹, and $\mu = 1.20 \times 10^{-4}$ s⁻¹ based on previously reported data on this system (30, 32).

In Fig. 5*E*, we plot the normalized fluorescence of cell in the device as a function of time after the inducers are added outside the living device. It takes around 2 h for different strains in the living sensor to show significant fluorescence (e.g., 0.5 of the maximum fluorescence). For the IPTG$_{RCV}$/GFP strain, the diffusion–induction-coupled model matches very well with experimental data (Fig. 5*E*).

Critical Timescales for Living Materials and Devices. From the above analysis, we know that the responsive time of a living material or device is determined by two critical timescales: the time for inducers to diffuse and accumulate around cells to the level that is sufficient for induction $t_{diffuse}$ and the time to induce GFP expression and reach a steady-state t_{induce}. To obtain analytical solutions for $t_{diffuse}$, we develop a simple but relevant model as illustrated in Fig. S10*A*. The model is similar to the geometry of the living sensor (Fig. 5*A*) but assumes that the cells are embedded in a segment of hydrogel close to the elastomer wall. The inducer concentration in the environment is taken to be constant I_0, and the total thickness of the hydrogel is L. By means of imaginary sources (33), the inducer concentration at location L (at the end of hydrogel) and time t can be expressed as $I(L, t)/I_0 = 2 \, erfc[L/(2\sqrt{D_g t})] - erfc[L/(\sqrt{D_g t})]$, where $erfc(x)$ is the complementary error function. From Fig. S10*B*, it can be seen that the simplified model can consistently represent the typical concentration profile in the cell chamber of the living sensor. From promoter activity expression, we assume that, only when the inducer concentration at a point reaches the level of K (i.e., $P = P_{max}/2$), the inducer concentration is sufficient to induce the cells. Therefore, the critical diffusion time for cells with a typical distance L from the environment is

$$t_{diffuse} = \left[\Lambda \left(\frac{K}{I_0} \right) \right]^{-2} \times \frac{L^2}{D_g}, \qquad \qquad [5]$$

where $\Lambda(x)$ is the inverse of function of $\Omega(x) = 2 \, erfc(x/2) - erfc(x)$, L^2/D_g is the typical diffusion timescale, and the prefactor $[\Lambda(K/I_0)]^{-2}$ accounts for the difference between I_0 and K. We further fit the prefactor into a power law that approximately gives $t_{diffuse} \approx 4/9/(I_0/K - 1)^{0.56} \times L^2/D_g$ (Fig. S11).

We next evaluate the timescale to induce the cell t_{induce}. When the inducer concentration around a cell reaches the level of K (i.e., P reaches the level of $0.5 P_{max}$), significant induction (e.g., expression of GFP) will occur in the cell. To solve Eqs. **3** and **4** analytically, we assume that the induction happens only after P reaches the level of $0.5 P_{max}$ and P maintains at a constant level (between $0.5 P_{max}$ and P_{max}) during the induction. Therefore, we can set $n = f = 0$ as the initial condition and P as a time-independent constant in Eqs. **3** and **4**. Further setting $C_n = C_f = 0$, we can obtain analytical solutions $n = P(1 - e^{-(m+\mu)t})/(m + \mu)$ for ^{n}GFP and $f = P(e^{-(m+\mu)t} - 1)/(m + \mu) - P(e^{-\mu t} - 1)/\mu$ for ^{f}GFP,

from which two characteristic timescales [i.e., $1/(m+\mu)$ and $1/\mu$] can be identified. Evidently, the characteristic timescale for the expression of ^{n}GFP is $1/(m+\mu)$. Because the maturation constant m is usually much larger than the growth constant μ (30, 34), the second term of ^{f}GFP has a much larger coefficient than the first term, and thus, the second term dominantly characterizes the expression of ^{f}GFP with a critical timescale of $1/\mu$. Therefore, we approximate the critical time to induce cells to reach steady-state fluorescence as

$$t_{induce} \approx \frac{1}{\mu}. \qquad [6]$$

Based on the known parameters for IPTG$_{RCV}$/GFP cells encapsulated in hydrogel at a typical distance of L (0.7 mm) from the environment, we can estimate the critical timescales of diffusion and induction to be 7.5 and 140 min, respectively. The induction of cells takes a much longer time than the transportation of inducers, which is consistent with the full model (Fig. 5 D and E). In total, the coupled diffusion–induction timescale is 2.4 h, which is also in good agreement with the full model's prediction (Fig. 5E).

The above analysis can provide a few guidelines for the design of future living materials. To design living materials and devices with faster responses, we need shorter times for both $t_{diffuse}$ and t_{induce}. To decrease $t_{diffuse}$ (Eq. 5), one can (i) reduce the thickness of the hydrogel, (ii) increase the diffusivity of inducer in the hydrogel, and (iii) increase the inducer concentration in the environment. However, to decrease t_{induce}, one can design cells with higher maturation constants or growth constants and add negative feedback into genetic circuit (31).

Conclusions

We have integrated genetically engineered cells as programmable functional components with stretchable, robust, and biocompatible hydrogel–elastomer hybrids to create a set of stretchable living materials and devices. These living materials and devices can be programmed with desirable functionalities by designing the genetic circuits in the cells as well as the structures and micropatterns of the hydrogel–elastomer hybrids. Moreover, we developed a quantitative model that accounts for the coupling between physical and biochemical processes in living materials. We further identified two critical timescales that determine the speed of response of the living materials and devices and provide guidelines for the design of future systems. This work has the potential to open technological avenues that capitalize on advances in synthetic biology and soft materials to implement stretchable, wearable, and portable living systems with important applications in the monitoring of human health (1) and environmental conditions (35) and the treatment and prevention of diseases (2).

Materials and Methods

All details associated with the materials, fabrication steps, and strain engineering appear in SI Text. Note that all procedures involving human subjects conformed to the guidelines for protecting the rights of human subjects and were approved by the Massachusetts Institute of Technology Committee on the Use of Humans as Experimental Subjects (COUHES protocol no. 1701827491). All subjects provided informed consent.

Briefly, different cell strains were picked from overnight growth on LB plates and cultured in LB with 50 μg/mL carbenicillin at 37 °C. Cell cultures (OD$_{600}$ ≈ 1) were infused into the patterned cavities between hydrogel and elastomer by metallic needles (Nordson EFD) through the hydrogel layer (Fig. S1). The holes induced by cell injection were sealed with small amounts of fast-curable pregel solution. The cell-contained device was washed with PBS three times followed by immersing the device in LB broth with carbenicillin and inducer(s) at 25 °C.

1. Pardee K, et al. (2014) Paper-based synthetic gene networks. *Cell* 159(4):940–954.
2. Mimee M, Tucker AC, Voigt CA, Lu TK (2015) Programming a human commensal bacterium, Bacteroides thetaiotaomicron, to sense and respond to stimuli in the murine gut microbiota. *Cell Syst* 1(1):62–71.
3. Friedland AE, et al. (2009) Synthetic gene networks that count. *Science* 324(5931):1199–1202.
4. Siuti P, Yazbek J, Lu TK (2014) Engineering genetic circuits that compute and remember. *Nat Protoc* 9(6):1292–1300.
5. Chen AY, et al. (2014) Synthesis and patterning of tunable multiscale materials with engineered cells. *Nat Mater* 13(5):515–523.
6. Florea M, et al. (2016) Engineering control of bacterial cellulose production using a genetic toolkit and a new cellulose-producing strain. *Proc Natl Acad Sci USA* 113(24):E3431–E3440.
7. Cheng AA, Lu TK (2012) Synthetic biology: An emerging engineering discipline. *Annu Rev Biomed Eng* 14:155–178.
8. Feinberg AW, et al. (2007) Muscular thin films for building actuators and powering devices. *Science* 317(5843):1366–1370.
9. Nawroth JC, et al. (2012) A tissue-engineered jellyfish with biomimetic propulsion. *Nat Biotechnol* 30(8):792–797.
10. Gerber LC, Koehler FM, Grass RN, Stark WJ (2012) Incorporation of penicillin-producing fungi into living materials to provide chemically active and antibiotic-releasing surfaces. *Angew Chem Int Ed Engl* 51(45):11293–11296.
11. Lee KY, Mooney DJ (2001) Hydrogels for tissue engineering. *Chem Rev* 101(7):1869–1879.
12. Zhao X, et al. (2011) Active scaffolds for on-demand drug and cell delivery. *Proc Natl Acad Sci USA* 108(1):67–72.
13. Seliktar D (2012) Designing cell-compatible hydrogels for biomedical applications. *Science* 336(6085):1124–1128.
14. Zhao X (2014) Multi-scale multi-mechanism design of tough hydrogels: Building dissipation into stretchy networks. *Soft Matter* 10(5):672–687.
15. Yuk H, Zhang T, Parada GA, Liu X, Zhao X (2016) Skin-inspired hydrogel-elastomer hybrids with robust interfaces and functional microstructures. *Nat Commun* 7:12028.
16. Gong JP, Katsuyama Y, Kurokawa T, Osada Y (2003) Double-network hydrogels with extremely high mechanical strength. *Adv Mater* 15(14):1155–1158.
17. Sun J-Y, et al. (2012) Highly stretchable and tough hydrogels. *Nature* 489(7414):133–136.
18. Yuk H, Zhang T, Lin S, Parada GA, Zhao X (2016) Tough bonding of hydrogels to diverse non-porous surfaces. *Nat Mater* 15(2):190–196.
19. Lin S, et al. (2014) Design of stiff, tough and stretchy hydrogel composites via nanoscale hybrid crosslinking and macroscale fiber reinforcement. *Soft Matter* 10(38):7519–7527.
20. Lee JN, Jiang X, Ryan D, Whitesides GM (2004) Compatibility of mammalian cells on surfaces of poly(dimethylsiloxane). *Langmuir* 20(26):11684–11691.
21. Darnell MC, et al. (2013) Performance and biocompatibility of extremely tough alginate/polyacrylamide hydrogels. *Biomaterials* 34(33):8042–8048.
22. Robb WL (1968) Thin silicone membranes–their permeation properties and some applications. *Ann N Y Acad Sci* 146(1):119–137.
23. Huh D, et al. (2010) Reconstituting organ-level lung functions on a chip. *Science* 328(5986):1662–1668.
24. Halldorsson S, Lucumi E, Gómez-Sjöberg R, Fleming RMT (2015) Advantages and challenges of microfluidic cell culture in polydimethylsiloxane devices. *Biosens Bioelectron* 63:218–231.
25. Jang K-I, et al. (2014) Rugged and breathable forms of stretchable electronics with adherent composite substrates for transcutaneous monitoring. *Nat Commun* 5:4779.
26. Yuk H, et al. (2017) Hydraulic hydrogel actuators and robots optically and sonically camouflaged in water. *Nat Commun* 8:14230.
27. Liao IC, Moutos FT, Estes BT, Zhao X, Guilak F (2013) Composite three-dimensional woven scaffolds with interpenetrating network hydrogels to create functional synthetic articular cartilage. *Adv Funct Mater* 23(47):5833–5839.
28. Dilanji GE, Langebrake JB, De Leenheer P, Hagen SJ (2012) Quorum activation at a distance: Spatiotemporal patterns of gene regulation from diffusion of an autoinducer signal. *J Am Chem Soc* 134(12):5618–5626.
29. Lin S, et al. (2016) Stretchable hydrogel electronics and devices. *Adv Mater* 28(22):4497–4505.
30. Leveau JH, Lindow SE (2001) Predictive and interpretive simulation of green fluorescent protein expression in reporter bacteria. *J Bacteriol* 183(23):6752–6762.
31. Alon U (2006) *An Introduction to Systems Biology: Design Principles of Biological Circuits* (CRC, Boca Raton, FL).
32. Kuhlman T, Zhang Z, Saier MH, Jr, Hwa T (2007) Combinatorial transcriptional control of the lactose operon of Escherichia coli. *Proc Natl Acad Sci USA* 104(14):6043–6048.
33. Fischer H, List E, Koh R, Imberger J, Brooks N (1979) *Mixing in Inland and Coastal Waters* (Academic, New York), pp 229–242.
34. Cubitt AB, et al. (1995) Understanding, improving and using green fluorescent proteins. *Trends Biochem Sci* 20(11):448–455.
35. Belkin S (2003) Microbial whole-cell sensing systems of environmental pollutants. *Curr Opin Microbiol* 6(3):206–212.